6748 *Macromolecules* **2009**, *42*, 6748–6760
DOI: 10.1021/ma900768p

Macromolecules
ARTICLE

Amphiphilic Graft Copolymers in Selective Solvents: Molecular Dynamics Simulations and Scaling Theory

Peter Košovan,[†] Jitka Kuldová,[†] Zuzana Limpouchová,[†] Karel Procházka,[†] Ekaterina B. Zhulina,[‡] and Oleg V. Borisov*[,‡,§]

[†]*Department of Physical and Macromolecular Chemistry, Faculty of Science, Charles University in Prague, Hlavova 8, 128 43 Prague, Czech Republic,* [‡]*Institute of Macromolecular Compounds, Russian Academy of Sciences, 199004 St. Petersburg, Russia, and* [§]*Institut Pluridisciplinaire de Recherche sur l'Environnement et les Matériaux, UMR 5254, UPPA CNRS, 64053, Pau, France*

Received April 8, 2009; Revised Manuscript Received June 17, 2009

ABSTRACT: Intramolecular structures in amphiphilic graft copolymers with hydrophilic side chains and hydrophobic backbone have been studied by molecular dynamics simulations. In accordance with earlier theoretical predictions [Borisov, O.; Zhulina, E. *Macromolecules* **2005**, *38*, 2506−2514], we have found that balance of repulsive and attractive intramolecular interactions may result in the pearl-necklace-type conformations. The globular "pearls" are formed by collapsed segments of the main chain comprising multiple spacers; these pearls are stabilized against aggregation by repulsive interactions of the hydrophilic grafts. The size of the pearls is controlled by the intramolecular hydrophilic−hydrophobic balance, whereas the total number of pearls in the graft copolymer depends on the length of the main chain. For graft copolymer with relatively long spacers we have observed intramolecular conformational transition from pearl-necklace structure to unimolecular cylindrical micelle upon a decrease in the solvent quality for the main chain. The results of simulations, in particular behavior of polymers of finite chain length, are rationalized on the basis of revised and extended scaling theory.

I. Introduction

Amphiphilic graft copolymers comprise multiple polymeric side chains end-grafted at regular intervals to a long main chain (backbone). When the spacers (segments of the main chain separating neighboring grafting points) are shorter than the grafts, these polymers are classified as molecular brushes. Recent advances in polymerization techniques have made possible synthesis of dense molecular brushes with chemically different main chain and the grafts and well-controlled molecular architecture, that is, with regular spacing and controlled molecular weights of the grafts.[1] These polymers have recently attracted considerable attention because of their interesting rheological behavior[2] and multiple potential applications in emerging domains of biomedical and nanotechnology.

The combination of topological complexity with amphiphilic nature of these copolymers enables one to exploit them as building blocks for diverse multidomain nanoscale structures emerging as a result of hierarchical intra- and intermolecular self-organization in selective solvents. These nanostructures may serve as nanocontainers, vector systems, molecular templates for nanowires, etc.

The steric repulsion between densely grafted side chains determines the most important conformational properties of the molecular brushes,[3,4] such as induced bending rigidity (enhanced apparent persistence length),[5,7] weak intermolecular penetration in semidilute solutions,[8] etc. Effects of the interactions between the grafts on local conformational structure of molecular brushes in good solvents were probed in SANS experiments,[9,10] which have demonstrated good agreement with theoretical predictions.

*Corresponding author. E-mail: borisov@univ-pau.fr.

Aqueous environment offers an excellent opportunity to tune independently solubility of chemically different main chain and of the grafts by using the thermosensitive polymer exhibiting the LCST behavior[17] as the backbone of the graft copolymer. In this case an increase in temperature leads to a decrease in solubility of the main chain and may trigger sequence of intramolecular conformational transitions.

In the case when the solvent is good for the grafts, but the main chain is poorly soluble, the collapse of the main chain may give rise to intramolecular micelles of various morphologies stabilized against aggregation due to repulsive interactions of the grafts. The interplay of the repulsive interaction among the grafts with the hydrophobic attraction among the main chain monomers is decisive for ability of the copolymers to assume diverse intramolecular structures.

The conformational behavior of the graft copolymers with poorly soluble backbone and grafts for which the solvent is good has been analyzed by means of scaling theory by Borisov and Zhulina.[18] It has been shown that a progressive decrease in the solvent quality for the main chain may provoke a sequence of morphological transitions between intramolecular aggregates of different morphologies, in particular formation of spherical or cylindrical intramolecular micelles and multidomain pearl-necklace structure comprising multiple spherical intramolecular micelles.

Similar pearl-necklace intramolecular structures have been proposed for hydrophobic linear polyelectrolytes[19] in salt-free solution, where they result from the balance of long-range Coulomb repulsion and short-range attractive interactions between the monomer units. The scaling theory for the graft copolymers in selective solvents[18] uses analogous arguments: Here the hydrophobic attraction of the monomer units of the main chain is counteracted by steric repulsive interactions among

 Published on Web 08/11/2009

the grafts. The former is short-ranged (on the length scale of the size of the monomer unit) while the latter operates on the length scale of the order of the size of the side chain. The multidomain intramolecular structures have been recently predicted theoretically and observed experimentally[20] for another type of amphiphilic graft copolymers, i.e., cylindrical core−shell molecular brushes formed by amphiphilic diblock copolymers grafted to the main chain by the terminal segment of the hydrophobic block. Here the cylindrical unimolecular micelle formed at moderately poor solvent quality conditions for the inner block exhibits longitudinal instability, leading to formation of pearl-necklace structures at lower solvent quality. Polymorphism of the intramolecular structures, including pearl necklaces, has been also observed in recent Monte Carlo simulations of amphiphilic multiblock copolymers in dilute solutions.[21]

The theoretical predictions of the formation of pearl-necklace structures have been subjected to thorough tests in computer simulations. At the beginning of the 2000s, several papers by Limbach and co-workers[11,12] appeared, confirming the existence of pearl necklaces in linear polyelectrolytes. In the paper of Košovan et al.[13] similar simulation results were confronted with earlier experimental results on fluorescence depolarization. Similar behavior may be observed when the side chains or both the backbone and the side chains are polyelectrolytes. Such systems have been studied in recent years by computer simulations. Košovan et al.[14] have studied comblike polymers with hydrophobic backbone and polyelectrolyte side chains. In this system the repulsion among the side chains is mostly provided by the electrostatics, but otherwise the simulation results have shown behavior qualitatively similar to that predicted by the theory for the neutral combs.[18] Comblike copolymers formed as interpolyelectrolyte complexes have been studied by Kramarenko et al.,[15] and more recently the same authors simulated polyelectrolytes with functional groups in the side chains.[16] Nevertheless, until now there has not been any systematic study which would confront the results of the scaling theory[18] with simulation results and analyze the validity of the predictions.

The aim of the present paper is to analyze intramolecular conformational transitions in amphiphilic graft copolymers by means of the molecular dynamics (MD) simulations and to confront the simulation results with the predictions of the scaling theory regarding the possibility of formation of intramolecular aggregates of different morphologies including necklace of the intramolecular starlike micelles and cylindrical structures.

The paper is organized as follows: In section II we introduce the computational model and method. The updated scaling theory of intramolecular structure formation in amphiphilic graft copolymers is outlined in section III. The simulation results are discussed in section IV. Finally, in section V we summarize our conclusions.

II. Computational Model and Method

Graft Copolymer Architectures. The simulated graft copolymer comprises multiple side chains regularly attached to the backbone. Its architecture is schematically shown in Figure 1. The number of monomer units in the backbone is $N_b = 320$ or $N_b = 500$. The backbone length has been chosen as a compromise between the large number of the main chain monomer units typical for experimental systems and required for observation of a well-defined intramolecular structures on one hand and limitations due to computer time on the other hand.

The grafting density is characterized by the ratio between unperturbed dimensions of an individual side chain and the average distance between neighboring grafts along the backbone, thus measuring the degree of overlap of the neighboring grafts. The corresponding scaling variable which quantifies the grafting density is defined below (see eq 11). In our simulations the grafting density is varied in such a way that for given values of the side chain length, n, and the backbone length, N_b, we vary systematically the spacing between the side chains, m. In particular, we have simulated graft copolymers with (i) side chains of length $n = 40$ and spacing $m = 4$ and $m = 8$ monomer units (densely grafted copolymers) and (ii) side chains of length $n = 5$ and spacings $m = 4$, 6, and 8 monomer units (sparsely grafted copolymers). The architectural parameters of the polymers are listed in Table 1.

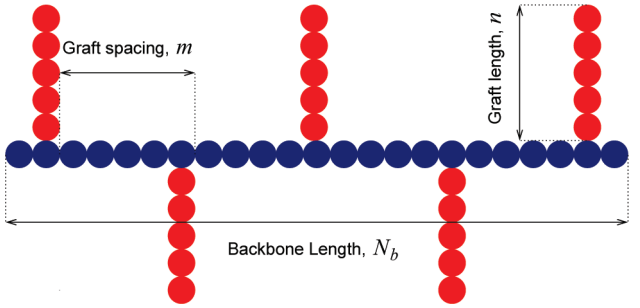

Figure 1. Schematic illustration of the graft copolymer architecture. Colors: main chain (backbone), blue; side chains (grafts), red.

Table 1. Architectures of Simulated Copolymers[a]

backbone length N_b	side-chain length n	side-chain spacing m	backbone hydrophobicity ε_{LJ}
320	40	4	0.3−2.0
320	40	8	0.3−1.4
320	5	4	0.6−1.5
320	5	6	0.6−1.5
320	5	8	0.6−1.5
500	5	6	1.2

[a] The backbone length, N_b, is the same for all systems. Two values of side-chain length, n, are used and for each of them a series of spacings, m. The empty row separates the systems with high (top) and low (bottom) grafting densities.

For each of the architectures, the interaction parameter ε_{LJ} which controls the solvent quality for the backbone was systematically varied in order to cover solvent quality ranging from close-to-theta solvent up to a very poor solvent. (The exact meaning of the ε_{LJ} parameter will be described in the following section after the interaction potentials will be introduced.)

Interaction Potentials and Parameters. We use the bead−spring model of the polymer with no restrictions on bond angles between the beads. Each bead may represent one or more monomer units, depending on how the model is mapped onto a real polymer. The simulation is performed in the dilute solution limit; i.e., we have one polymer molecule in the simulation box. The box is larger than any of the dimensions of the molecule.

The polymer contains two types of monomer units: hydrophobic ones in the backbone and hydrophilic ones which form the grafts. For the interaction between hydrophilic monomer units of the side chains we use only the repulsive part of the LJ potential, also known as the Weeks−Chandler−Andersen or WCA potential:

$$U'_{LJ} = \begin{cases} 4\varepsilon'_{LJ}\left[\left(\frac{\sigma'_{LJ}}{r}\right)^{12} - \left(\frac{\sigma'_{LJ}}{r}\right)^{6}\right] + \varepsilon'_{LJ} & \text{for } r \le R'_c \\ 0 & \text{for } r \ge R'_c \end{cases} \quad (1)$$

where we set $\varepsilon'_{LJ} = 1.0$, $\sigma'_{LJ} = 1.0$, and the interaction cutoff $R'_c = 2^{1/6}\sigma'_{LJ}$. The same interaction potential is used for the

cross-interaction between the hydrophilic and hydrophobic units. The interactions between hydrophobic monomer units of the backbone are modeled by the Lennard-Jones potential (LJ)

$$U_{\mathrm{LJ}} = \begin{cases} 4\varepsilon_{\mathrm{LJ}}\left[\left(\frac{\sigma_{\mathrm{LJ}}}{r}\right)^{12} - \left(\frac{\sigma_{\mathrm{LJ}}}{r}\right)^{6} + c(R_{\mathrm{c}})\right] & \text{for } r \le R_{\mathrm{c}} \\ 0 & \text{for } r \ge R_{\mathrm{c}} \end{cases} \quad (2)$$

with a shift of $c(R_{\mathrm{c}}) = (\sigma_{\mathrm{LJ}}/R_{\mathrm{c}})^6 - (\sigma_{\mathrm{LJ}}/R_{\mathrm{c}})^{12}$ and the cutoff radius $R_{\mathrm{c}} = 2.5\sigma_{\mathrm{LJ}}$. We fix the monomer size by setting $\sigma_{\mathrm{LJ}} = 1.0$. The depth of the minimum of the potential is controlled by the value of the $\varepsilon_{\mathrm{LJ}}$ parameter. Its magnitude determines the hydrophobicity (solvent quality) for the hydrophobic monomer units. As a reference for the scale of solvent quality, we use the result of Micka, Holm, and Kremer,[22] who have determined that for the polymer model with the same interaction parameters as we use here $\varepsilon_{\mathrm{LJ}} = 0.34 \pm 0.02$ corresponds to the Θ solvent conditions. In the simulations presented here we use $\varepsilon_{\mathrm{LJ}} = 0.60-2.0$, which is in the poor solvent regime. We do not go beyond the maximum value of $\varepsilon_{\mathrm{LJ}} = 2.0$ because of the technical limitations of the simulations: systems with higher values of $\varepsilon_{\mathrm{LJ}}$ tend to be trapped in kinetically frozen states and do not relax to equilibrium on time scales accessible to our simulations.

Chemical bonds (connectivity) along the polymer backbone are modeled by the finite-extension nonlinear elastic (FENE) potential

$$U_{\mathrm{FENE}} = -\frac{1}{2} K_{\mathrm{FENE}} R_{\mathrm{FENE}}^2 \ln\left(1 - \left(\frac{r}{R_{\mathrm{FENE}}}\right)^2\right) \quad (3)$$

where we set the stiffness constant $K_{\mathrm{FENE}} = 7.0$ and the cutoff radius $R_{\mathrm{FENE}} = 2.0$. These values, combined with the L-J potential, ensure the average bond length about $1.0\sigma_{\mathrm{LJ}}$. For a more detailed discussion of the potentials and the meaning of their parameters we refer the reader to the book of Binder[23] and references therein.

Simulation Method. We are using the molecular dynamics (MD) simulation method with the Langevin thermostat.[24] It involves the solution of classical Newtonian equations of motion, which include two additional forces:

$$m_i \frac{\mathrm{d}^2 \mathbf{r}_i}{\mathrm{d}t^2} = -\nabla \sum_{j \neq i} U(r_{ij}) + \mathbf{F}_i^{\mathrm{D}} + \mathbf{F}_i^{\mathrm{R}} \quad (4)$$

where $\mathbf{r}_i$ is the position vector of ith particle, m_i is its mass, t is time, and $U(r)$ is the interaction potential. The dissipative force $\mathbf{F}_i^{\mathrm{D}}$ and the random force $\mathbf{F}_i^{\mathrm{R}}$ emulate the collisions with solvent molecules which are not simulated explicitly. The two forces are defined by the following relations

$$\mathbf{F}_i^{\mathrm{D}} = -m\Gamma \frac{\mathrm{d}\mathbf{r}_i}{\mathrm{d}t} \quad (5)$$

$$\langle \mathbf{F}_i^{\mathrm{R}}(t) \cdot \mathbf{F}_i^{\mathrm{R}}(t') \rangle = 6\Gamma k_{\mathrm{B}} T m \delta_{ij} \delta(t - t') \quad (6)$$

$$\langle \mathbf{F}_i^{\mathrm{R}}(t) \rangle = 0 \quad (7)$$

where k_{B} is the Boltzmann constant and Γ is the coupling constant of the heat bath. The use of the implicit solvent allows us to reduce the number of degrees of freedom of the simulated system and thus to simulate much longer times in comparison with explicit solvent models. The simulations were performed using the ESPResSo software package.[25,26]

Having set the monomer size as $\sigma_{\mathrm{LJ}} = \sigma'_{\mathrm{LJ}} = 1.0$, it is convenient to use it as a natural (reduced) unit of length. We fix temperature by setting $k_{\mathrm{B}}T = 1.0$ and measure energy in units of $k_{\mathrm{B}}T$. Time is measured in the standard Lennard-Jones units of time, $t^* = \sigma_{\mathrm{LJ}}(m/k_{\mathrm{B}}T)^{1/2}$. The integration of the equations of motion is performed with the time step $\Delta t = 0.0125\ t^*$ and the thermostat coupling constant $\Gamma = 1.0\ t^{*-1}$. A typical simulation lasts about $5 \times 10^5\ t^*$, out of which about $1 \times 10^5\ t^*$ are discarded as equilibration and in the rest of the simulation the conformations are sampled every $250\ t^*$.

III. Scaling Theory of Intramolecular Structures in Amphiphilic Graft Copolymers

Following the scaling approach developed in ref 18, we describe below different intramolecular structures emerging in amphiphilic graft copolymers as a result of conformational transition induced by a decrease of the solvent quality for the backbone. In the scaling analysis, we assume that both the grafts and the spacers are flexible and comprise n and m monomer units of equal size, respectively (see also schematic illustration in Figure 1). The size of the monomer unit (controlled by σ_{LJ} in simulations) is used as a unit of length. The good solvent quality for the monomer units of the grafts is characterized by the excluded volume parameter (second virial coefficient normalized by the cube of the monomer unit length) $v \approx 1$. The poor solvent quality for the backbone can be quantified by the Flory−Huggins parameter $\chi \ge \chi_\theta \equiv 1/2$. The latter can be quantitatively related to the parameter $\varepsilon_{\mathrm{LJ}}$ used in our simulations, which determines the strength of the monomer−monomer attraction and thus is the measure for the monomer hydrophobicity. In the vicinity of the theta-point, $\chi - 1/2 \ll 1$, it is convenient to introduce the thermal blob size, $\xi_t \sim (\chi - 1/2)^{-1}$, which is proportional to the correlation length of density fluctuations in a polymer globule.[27] Close to the theta-point all the local properties of the polymer globule can be presented as power-law functions of ξ_t: The concentration of monomer units in a polymer globule formed by infinitely long chain is $\tau \cong \xi_t^{-1}$. The free energy per monomer unit in a large globule scales as $\mu \cong -k_{\mathrm{B}}T\xi_t^{-2} \cong -k_{\mathrm{B}}T\tau^2$, whereas the excess free energy of the globule−solvent interface (per unit area) is given by

$$\gamma \cong k_{\mathrm{B}}T\xi_t^{-2} \cong k_{\mathrm{B}}T\tau^2 \quad (8)$$

The extensional force that is necessary to apply to the chain ends in order to unfold the collapsed polymer globule[28] scales as $f/k_{\mathrm{B}}T \cong (-\mu/k_{\mathrm{B}}T)^{1/2} \cong \xi_t^{-1} \cong \tau$.

This universality breaks down for strongly hydrophobic polymer when $(\chi - 1/2) \ge 1$. In this regime, which is most relevant in our simulations, the density of the collapsed globule asymptotically approaches the value of the order of unity, $\tau(\chi) \to 1$, whereas $\mu(\chi)$ and $\gamma(\chi)$ remain increasing functions of χ; that is, they increase upon an increase in the hydrophobicity of the main-chain monomer units.[29]

Collapse Transition and Intramolecular Structures in Densely Grafted Copolymers. We start with outlining scaling theory predictions for the intramolecular structures arising in densely grafted copolymers (molecular brushes) as a result of collapse of the main chain. We distinguish three main scaling regimes for densely grafted copolymer depending on the range of the solvent quality: in the theta-regime the backbone remains uniformly stretched whereas two other regimes (with confined and nonconfined intramolecular micelles) correspond to locally collapsed conformations of

the main chain of the molecular brush, Figure 2. The theta-regime and the regime of nonconfined micelles have been discussed in detail in refs 3 and 18, and we only briefly outline predictions of the theory with respect to the graft copolymer conformations in these regimes. Here we present a more comprehensive analysis of the structure of the molecular brush in the vicinity of the onset of the collapse transition (i.e., in the regime of confined intramolecular micelles) as compared to our previous consideration in ref 18.

1. Graft Copolymer under Theta-Solvent Conditions for the Main Chain. As has been discussed in ref 3 under theta-solvent conditions for the main chain, the balance of repulsive interactions of the grafts and entropic elasticity of the backbone results in equilibrium stretching of both the grafts and the spacers. The grafts are stretched to the size

$$D_\theta \cong n^{3/5} v^{1/5} \zeta^{5/21} \tag{9}$$

and the size of the stretched spacers is

$$h_\theta \cong m^{1/2} \zeta^{5/21} \tag{10}$$

where following ref 18 we have introduced the scaling parameter

$$\zeta = \frac{n^{3/5} v^{1/5}}{m^{1/2}} \tag{11}$$

characterizing density of grafting of the side chains to the backbone: $\zeta \gg 1$ for densely grafted copolymers, $n \gg m$, whereas for sparsely grafted copolymers, $n \leq m$, one finds $\zeta \leq 1$. (We draw the attention of the reader to the fact that in ref 18 the symbol γ was used instead of ζ for the same scaling parameter. Here and below we use γ to denote the excess interfacial free energy.) The elastic tension arising in the main chain is given by

$$\frac{f_\theta}{k_B T} \cong m^{-1/2} \zeta^{5/21} \tag{12}$$

Each spacer can be envisioned as a string of elastic blobs[30] of size $\xi_\theta \sim k_B T/f_\theta$. Since the blobs are Gaussian, each of them comprises $g_\theta \cong \xi_\theta^2 \cong m\zeta^{-10/21}$ monomer units. Hence, the number of elastic blobs per spacer $m/g_\theta \cong \zeta^{10/21} \gg 1$, provided that $\zeta \gg 1$, which specifies conditions of strong stretching of spacers.

On a large scale the graft copolymer behaves as a self-avoiding wormlike chain characterized by an effective contour length $L \cong (N_b/m)h$, effective thickness D, and effective (apparent) persistence length.[5-7]

2. Necklace of Confined Intramolecular Micelles. The onset of collapse transition in the stretched backbone is specified by the condition $\xi_t \leq \xi_\theta$, which occurs at $\tau \geq \tau_c$, where

$$\tau_c \cong m^{-1/2} \zeta^{5/21} \tag{13}$$

Hence, the collapse transition in the molecular brush is shifted significantly into the range of poor solvent conditions as compared to the onset of the coil-to-globule transition in the main chain without grafts ($\tau \geq N_b^{-1/2}$) and even to that in a single spacer alone ($\tau \geq m^{-1/2}$). The magnitude of the shift is controlled by the grafting density parameter ζ.

At $\tau \geq \tau_c$ the main chain of the molecular brush is locally collapsed, whereas on the large scale the macromolecule retains the wormlike chain conformation. In this regime we anticipate formation of a pearl-necklace structure of the starlike intramolecular micelles consisting of globular

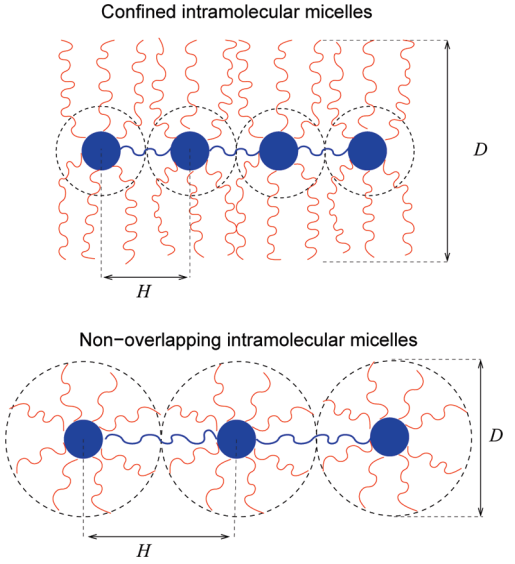

Figure 2. Schematic illustration of the necklace of confined (top) and nonoverlapping (bottom) intramolecular micelles. Colors: main chain (backbone), blue; side chains (grafts), red.

domains, each comprising p_c collapsed spacers and decorated by a corona formed by the same number of grafts. The collapsed globular domains are separated by bridges; each bridge comprises p_b spacers. Then $p = p_b + p_c$ is the total number of grafts per period of the structure along the backbone (per one intrachain micelle). The total number of micelles in the chain is $N_b/(m(p_c + p_b))$.

If $h(\tau)$ be the average axial distance per one graft, then the axial length of the brush per micelle is $H(\tau) = ph(\tau)$. We assume (and this will be proven below) that at $\tau_c \leq \tau \leq \tau^*$, where

$$\tau^* \cong m^{-1/2} \zeta^{25/27} \tag{14}$$

the axial length of the brush per micelle, $H = h(p_c + p_b)$, is smaller than the brush thickness D, which implies strong longitudinal confinement of the intramolecular micelles.

The free energy of the chain of confined intramolecular micelles can be presented as

$$F(h, p_c, p_b) = F_{corona} + F_{interface} + F_{bridge} \tag{15}$$

where the first term describes excluded volume interactions between the grafts, the second term accounts for the excess free energy of the interface between collapsed globular cores of the intramolecular micelles and the surrounding solution, and the last term describes free energy of the segments of the main chain forming the bridges.

The coronal contribution to the free energy (in $k_B T$ units) per one intrachain micelle can be calculated following ref 31 as the number of coronal blobs by integrating local number density of the blobs $\xi^{-3}(r)$ over the volume of the corona:

$$\left(\frac{F_{corona}}{k_B T}\right)_{\text{per micelle}} \cong \int_{R_{core}}^{H} \frac{r^2\, dr}{\xi_{3d}^{\,3}(r)} + \int_{H}^{D} \frac{Hr\, dr}{\xi_{2d}^{\,3}(r)} \tag{16}$$

Here $\xi_{3d}(r) \cong r/p_c^{1/2}$ is the size of the blob at distance r from the center of the core domain in the central nonconfined region of the corona, $R_{core} \leq r \leq H$, where it preserves the same spherically symmetric structure as in a spherical starlike micelle.[31,32] In the confinement region, $H \leq r \leq D$, where the corona acquires cylindrical symmetry, the blob size is given by[33] $\xi_{2d}(r) \cong (Hr/p_c)^{1/2}$.

After performing integration in eq 16, we obtain

$$\left(\frac{F_{\text{corona}}}{k_{\text{B}}T}\right)_{\text{per micelle}} \cong p_{\text{c}}^{3/2} \ln\left(\frac{H}{R_{\text{core}}}\right) + p_{\text{c}}^{3/2}\left[\left(\frac{D}{H}\right)^{1/2} - 1\right] \tag{17}$$

In the strong confinement regime, $D \gg H$, the extension of the coronal chains, D, is given by the same expression as in longitudinally uniform cylindrical brush

$$D(h) \cong n^{3/4} v^{1/4} h^{-1/4} \tag{18}$$

that leads with the account of the relation $H = hp$ and under the assumption that $p_{\text{c}} \gg p_{\text{b}}$ to the final expression for the coronal free energy

$$\left(\frac{F_{\text{corona}}}{k_{\text{B}}T}\right)_{\text{per micelle}} \cong p_{\text{c}}^{3/2} \ln \frac{H}{R_{\text{core}}} + (p_{\text{c}} + p_{\text{b}}) n^{3/8} v^{1/8} h^{-5/8} \tag{19}$$

The first term in eq 19 describes the contribution from quasi-spherical region of the corona, which is proximal to the core and unperturbed by confinement, whereas the second term describes the distal region which retains cylindrical brush structure and accounts for the contribution from both the grafts forming the coronas of the intrachain micelles and those belonging to the bridges.

The excess free energy of the interface of collapsed globular core of the size $R_{\text{core}} \cong (p_{\text{c}} m/\tau)^{1/3}$ is given by

$$\left(\frac{F_{\text{interface}}}{k_{\text{B}}T}\right)_{\text{per micelle}} \cong \frac{\gamma}{k_{\text{B}}T}\left(\frac{p_c m}{\tau}\right)^{2/3} \tag{20}$$

The free energy of a segment of the main chain bridging the cores of two neighboring intrachain micelles can be presented as

$$\left(\frac{F_{\text{bridge}}}{k_{\text{B}}T}\right)_{\text{per micelle}} \cong \frac{(p_{\text{c}} + p_{\text{b}})^2 h^2}{p_{\text{b}} m} + p_{\text{b}} m \tau^2 \tag{21}$$

where the first term describes conformational free energy of the stretched bridge and the second term accounts for the increase in the free energy of the excluded volume interactions of a segment of the main chain upon its transfer from the bulk of the collapsed hydrophobic domain to the stretched bridge, that is, into poor solvent. (We remind the reader that $\mu/k_{\text{B}}T \cong -\tau^2$ corresponds in volume approximation to the free energy of a monomer unit in collapsed globule.[27])

Finally, the total free energy of the graft copolymer is presented as

$$\frac{F}{k_{\text{B}}T} = \frac{N_{\text{b}}}{m}\left(\frac{1}{p_{\text{c}} + p_{\text{b}}}\left[\frac{\gamma}{k_{\text{B}}T}\left(\frac{p_{\text{c}} m}{\tau}\right)^{2/3} + p_{\text{c}}^{3/2} \ln \frac{H}{R_{\text{core}}}\right] + n^{3/8} v^{1/8} h^{-5/8} + \frac{(p_{\text{c}} + p_{\text{b}}) h^2}{p_{\text{b}} m} + \frac{p_{\text{b}} m \tau^2}{p_{\text{c}} + p_{\text{b}}}\right) \tag{22}$$

Minimization of the free energy, eq 22, with respect to p_{b} under the assumption that $p_{\text{b}} \ll p_{\text{c}}$ gives

$$\frac{p_{\text{b}}}{p_{\text{c}} + p_{\text{b}}} \cong \frac{h}{m\tau} \tag{23}$$

and, correspondingly, the contribution of bridges to the overall free energy scales as

$$\frac{F_{\text{bridge}}}{k_{\text{B}}T} \cong \frac{N_{\text{b}}}{m} h\tau \tag{24}$$

Minimization of the free energy with respect to h leads to the relation

$$\tau \cong n^{3/8} v^{1/8} h^{-13/8} \tag{25}$$

or

$$h(\tau) = h_\theta \left(\frac{\tau}{\tau_{\text{c}}}\right)^{-8/13}$$

Hence, the average axial distance between the grafts is controlled by repulsive interactions in the peripheral cylindrical region of the confined coronas of intramolecular micelles.

Minimization with respect to p_{c} provides the expression for the number of spacers involved in one collapsed domain:

$$p_{\text{c, opt}} \cong \gamma^{6/5} (m/\tau)^{4/5} \left(\ln \frac{H}{R_{\text{core}}}\right)^{-6/5} \tag{26}$$

which is, with the accuracy of logarithmic prefactor, identical to that in a starlike spherical micelle formed by diblock copolymers with n and m monomer units forming the hydrophilic and the hydrophobic blocks, respectively.[32] Hence, the aggregation number is controlled mostly by repulsive interactions between the grafts in the quasi-spherical region of the corona which is proximal to the core. The size of the collapsed hydrophobic core is given by

$$R_{\text{core}} \cong (p_{\text{c}} m/\tau)^{1/2} \cong \gamma^{2/5} (m/\tau)^{3/5} \tag{27}$$

The number of spacers included in bridges (per period) can be calculated as

$$p_{\text{b}} \cong \frac{h(\tau)(p_{\text{c}} + p_{\text{b}})}{m\tau} \cong p_{\text{c}} \zeta^{5/13} (m\tau^2)^{-21/26} \tag{28}$$

where we have assumed that $p_{\text{b}} \leq p_{\text{c}}$.

According to eq 26, a decrease in the solvent quality (an increase in τ) leads to an increase in the aggregation number and, consequently, to a decrease in the number of intramolecular micelles in the chain. Simultaneously, an axial dimension of the micelle, $H = h_{\text{p}}$, increases. Although the thickness of the molecular brush D also increases as a function of τ, the ratio $H/D \cong (\tau/\tau^*)^{27/13}$ grows as a function of τ and becomes of the order of unity at

$$\tau \cong \tau^* \cong m^{-1/2} \zeta^{25/27} \tag{29}$$

which corresponds to vanishing confinement of the intramolecular starlike micelles. Remarkably, the ratio $\tau^*/\tau_{\text{c}} \cong \zeta^{130/189}$; hence, the regime of confined micelles can be observed only for high grafting densities (large values of ζ).

It is instructive to compare the number of spacers, p_{c}, included in the core domain of one micelle and the number p_{b} of spacers forming bridges connecting it to the neighboring intramolecular micelles. As follows from eq 28

$$p_{\text{b}}/p_{\text{c}} \cong \zeta^{5/13} (m\tau^2)^{-21/26} \tag{30}$$

As follows from eq 30, at the onset of formation of intramolecular micelles, $\tau \cong \tau$, the numbers of spacers in collapsed domains and in the bridges are approximately equal, $p_c \cong p_b \cong \zeta^{5/21}$. For realistic values of ζ this implies the values of the order of unity. The ratio p_c/p_b progressively increases as a function of τ and at crossover to the regime of nonoverlapping micelles, $\tau \cong \tau^*$, we find $p_c/p_b \cong \zeta^{10/9} \gg 1$; that is, the majority of segments of the backbone are concentrated in the collapsed micellar cores. We note that due to extended scaling analysis presented above the diagram of states in ref 18 is slightly modified: regions II and III merge in a single region of confined micelles with the parameters summarized in Table 2.

3. Nonoverlapping Intramolecular Micelles. The regime of nonconfined starlike intramolecular micelles was discussed in details in ref 18. Here we only outline the main results. At $\tau \geq \tau^*$ the molecular brush can be presented as a necklace of spherical intramolecular micelles with virtually nonoverlapping starlike coronas. The aggregation number in nonconfined micelles is given by eq 26, but with the logarithmic factor $(\ln D/R_{core})^{-6/5}$ since at $\tau \geq \tau^*$ the distal cylindrically symmetrical region of the corona disappears and the free energy of the corona is given by $F_{corona}/k_BT \cong p^{1/2} \ln(D/R_{core})$. Hence, in this regime the number of spacers per one intramolecular micelle increases whereas the number of micelles in the molecular brush decreases upon a decrease in the solvent quality as well as in the regime of confined intramolecular micelles. The radius of the corona (which coincides with the distance between neighboring micelles) is given by $D_{corona} \cong n^{3/5}\upsilon^{1/5}p^{1/5} \cong n^{3/5}\upsilon^{1/5}\gamma^{6/25}(m/\tau)^{4/25}$ and exceeds by far the size of the core $R_{core} \cong (m/\tau)^{3/5}\gamma^{2/5}$. The repulsive force arising upon overlap of the coronas $f \cong F_{corona}/D$ exceeds tension $\sim k_BT\tau$ in the bridges connecting globular domains, which ensures only marginal overlap of the micellar coronas.

4. Finite-Size Effects. In the above-presented analysis of the evolution of conformations of graft copolymers in course of the collapse, we implicitly assumed that the number of grafts (and spacers) in the copolymer is sufficiently large. In this case, the local conformational structure of the copolymer is not affected by the length of the backbone and the end effects are negligible. Indeed, as we have discussed above, the free energy per one spacer involved in the formation of the spherical intramolecular micelle, eq 15, exhibits a sharp minimum as a function of the aggregation number p. The optimal aggregation number $p = p_{opt}$ corresponding to this minimum is given by eq 26. In the case of $N_b/(p_{opt}m) \gg 1$ variation in the number of micelles in the chain (which can assume only integer values) corresponds to fairly continuous variation of the number of spacers per micelle. The number of intramolecular micelles and the number of spacers in each micelle experience thermal fluctuations around the optimal values. However, relative fluctuations in the number of micelles (and in all the large scale properties like R_g and R_h) are small; all the micelles comprise fairly equal numbers of spacers $p \approx p_{opt}$.

Below we briefly discuss the finite size effects arising in graft copolymers with relatively short backbones and/or large aggregation numbers in optimal micelles, $N_b/(mp_{opt}) \sim 1$. If this number is not close to an integer, the chain cannot assume a configuration of necklace of micelles with *equal* aggregation numbers close to the optimal ones. As a result, the minimal free energy may correspond either to a necklace of micelles with equal but nonoptimal ($p \geq p_{opt}$ or $p \leq p_{opt}$) aggregation numbers or to a necklace comprising micelles with significantly different aggregation numbers.

Consider first the situation $1 \leq N_b/(p_{opt}m) \leq 2$, which for a given N_b, n, m corresponds to a certain range of variation of ε_{LJ}. From the symmetry reason, it is clear that in this range of parameters the graft copolymer molecule either forms one intramolecular micelle with aggregation number $p \geq p_{opt}$ or splits into two micelles with $p \leq p_{opt}$. The transition from one to two micelles occurs at a certain value of $\varepsilon_{LJ}(tr)$ corresponding to a particular value of the ratio $N_b/(mp_{opt})$ (simple analysis based on harmonic approximation for the free energy $F(p)$ leads to the value of 4/3 for this ratio in the transition point). In the vicinity of the transition point the copolymer chain samples with approximately equal probabilities the states with one and two intrachain micelles. As a result, its size and shape experience strong fluctuations (relative fluctuations of the order of unity).

Table 2. Scaling Dependencies for Local Conformational Properties of the Densely Grafted, $\zeta \geq 1$, Copolymers in Different Regimes Corresponding to Variation in the Solvent Quality for the Main Chain

regime	θ	confined micelles	nonconfined micelles
τ	$\tau < \tau_c$	$\tau_c < \tau < \tau^*$	$\tau > \tau^*$
p_c		$(m\tau^2)^{4/5}$	$(m\tau^2)^{4/5}$
p_b		$\zeta^{5/13}(m\tau^2)^{-1/130}$	$n^{3/5}\upsilon^{1/5}m^{-21/25}\tau^{-17/25}$
h	∞	$m^{5/26}\tau^{-8/13}\zeta^{5/13}$	$n^{3/5}\upsilon^{1/5}(m\tau^2)^{-16/25}$
H	$m^{1/2}\zeta^{5/21}$	$m^{129/130}\tau^{64/65}\zeta^{5/13}$	$n^{3/5}\upsilon^{1/5}(m\tau^2)^{4/25}$
D	$n^{3/5}\upsilon^{1/5}\zeta^{5/21}$	$(n^{3/5}\upsilon^{1/5})^{15/13}\tau^{2/13}$	$n^{3/5}\upsilon^{1/5}(m\tau^2)^{4/25}$
f/k_BT	$m^{-1/2}\zeta^{5/21}$	τ	τ

Further decrease in the main-chain hydrophobicity brings the system to the situation $2 \leq N_b/(p_{opt}m) \leq 3$. In this range of ε_{LJ} the transition from the conformation with two micelles with $p > p_{opt}$ to the conformation with three micelles, two larger ones at the ends of the chain and one smaller in the middle of the chain, occurs. Again, relative fluctuations in R_g and R_h near the transition point where conformations with different numbers of micelles coexist are of the order of unity, though less dramatic than those accompanying splitting of a single intramolecular micelle.

Cascade of the conformational transitions related to an increase in the number of intramolecular micelles is accompanied by progressively decreasing peaks in the relative fluctuations of the chain size, reflecting coexistence of conformations with different numbers of micelles.

Intramolecular Structures in Sparsely Grafted Copolymers. Similarly to diblock copolymers with long hydrophobic blocks capable of self-assembly into nanostructures of diverse morphologies,[34,35] graft copolymers with sufficiently long hydrophobic spacers are expected to exhibit polymorphism of the intramolecular structures.[18] In both cases so-called crew-cut aggregates of different shape characterized by relatively large hydrophobic domains decorated by thin hydrophilic coronas are formed.

The driving force for the morphological transition is the gain in conformational entropy of the extended core-forming blocks (spacers) penalized by an increase in the repulsive interactions in the hydrophilic coronas of the aggregates upon transformation of spherical micelles to cylindrical ones and further to quasi-planar (vesicles, discs) structures. Hence, the sequence of the sphere-to-cylinder and cylinder-to-disc (vesicle) transitions can be provoked by a decrease in hydrophilic/hydrophobic balance caused, e.g., by decreasing solubility of the corona-forming chains or by increasing hydrophobicity of the core-forming blocks.

Quantitatively, the condition $\zeta \leq 1$ has to be fulfilled to enable formation of cylindrical intramolecular micelles in a certain range of the solvent quality conditions for the

main chain. The range of thermodynamic stability of the cylindrical intramolecular aggregates is given by

$$m^{1/2}\zeta^5 \frac{k_B T \tau^3}{\gamma} \cong 1 \tag{31}$$

The latter equation specifies (with different numerical prefactors) the transition lines (binodals) at which cylindrical unimolecular micelles coexist in equilibrium with a necklace of spherical intramolecular micelles or with discs (vesicles). As follows from eq 31, fusion of intramolecular spherical micelles into a cylindrical unimolecular micelle is predicted to occur upon a decrease in parameter ζ, which may be induced (for a fixed copolymer composition) by a decrease in the excluded volume repulsive interactions of the coronal chains. Analogous morphological transitions in diblock copolymer micelles induced by variation in the quality of repulsive interactions in the corona have been studied in ref 34.

Alternatively, the variation of the ratio τ^3/γ as a result of the change in hydrophobicity of the main-chain monomers may provoke transition between intramolecular structures of different morphologies. As discussed in the beginning of this section, in the vicinity of the theta-point, $\chi - 1/2 \ll 1$, the scaling relation $\gamma/k_B T \sim \tau^2$ holds and the ratio τ^3/γ is an increasing function of χ. On the contrary, at $\chi - 1/2 \geq 1$, the density of the collapsed polymer globule approaches the limit of $\tau \sim 1$ whereas γ increases and the τ^3/γ ratio decreases as a function of χ. Hence, we conclude that an increase in χ may provoke the transition from a necklace of spherical micelles to a unimolecular cylindrical micelle provided the main chain of the graft copolymer is sufficiently long.

IV. Simulation Results and Discussion

All the performed simulations clearly indicate progressive collapse of the graft copolymer molecules when the hydrophobicity of the backbone increases. This behavior is common for both the systems with low and high grafting densities. It can be seen from the dependencies of the hydrodynamic radius, R_h, on solvent quality for the backbone (quantified by parameter ε_{LJ}). They are presented in Figure 3 (high grafting density) and in Figure 4 (low grafting density). The hydrodynamic radius was calculated using the expression for the Zimm model in Kirkwood−Riseman approximation.[36] The dependence of R_g on ε_{LJ} (not shown) qualitatively follows the same trend with slightly larger fluctuations and error bars. The variation of the ratio R_g/R_h is plotted as a function of ε_{LJ} in Figure 5 for the high grafting density and in Figure 6 for the low grafting density. A decrease in the R_g/R_h ratio as a function of ε_{LJ} indicates progressive variation in the shape of the macromolecule as a whole in the course of the collapse induced by the decrease in the solvent quality for the backbone.

Figure 7 shows the average stretching (end-to-end distance) of the side chains for the systems with high grafting density. It shows that although the polymer molecule as a whole collapses and its dimensions decrease with increasing ε_{LJ}, the steric repulsion among the side chains increases, which causes increasing stretching of the side chains with increasing hydrophobicity of the backbone.[37]

However, an analysis of collective variables such as R_g or R_h does not enable us to trace the sequence of intramolecular conformational transitions predicted by theory. Therefore, before performing a detailed numerical analysis of the evolution of the intramolecular structure as a function ε_{LJ}, we illustrate typical observed conformations using simulation snapshots. Figure 8 shows snapshots of a selected polymer with high grafting density

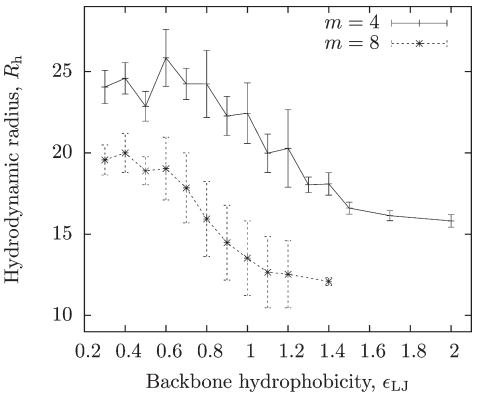

Figure 3. Variation of the hydrodynamic radius, R_h, with the change of the solvent quality for the backbone (ε_{LJ}, eq 2) for copolymers with high density of grafts (see Table 1).

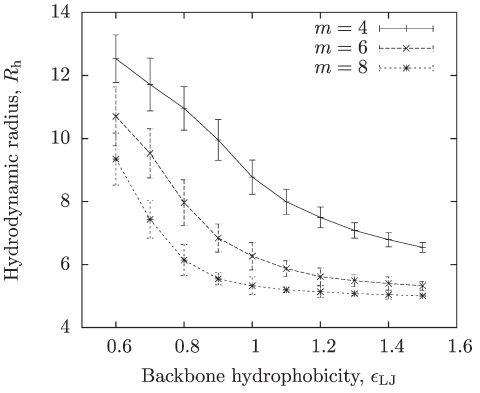

Figure 4. Variation of the hydrodynamic radius, R_h, with the change of the solvent quality for the backbone (ε_{LJ}, eq 2) for copolymers with low density of grafts (see Table 1).

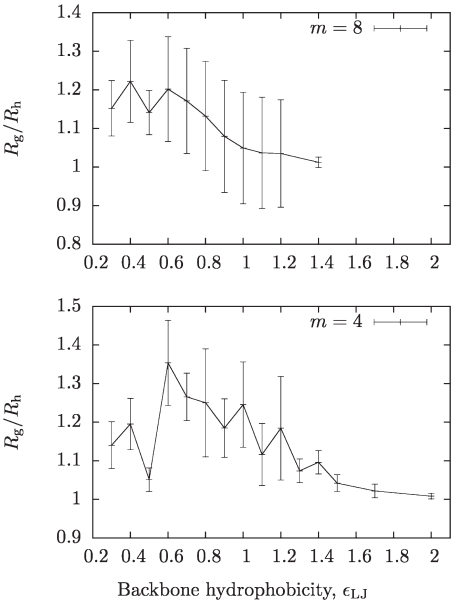

Figure 5. Variation of the ratio R_g/R_h with the change of the solvent quality for the backbone (ε_{LJ}, eq 2) for copolymers with high density of grafts (see Table 1).

(side-chain length $m = 40$ and spacer length $n = 8$). For densely grafted polymers the theory predicts that upon decreasing solvent quality for the backbone (increasing ε_{LJ}) the macromolecule

acquires a pearl-necklace-type conformation. The pearl size is increasing whereas the number of pearls is decreasing with increasing ε_{LJ}. This is perfectly confirmed by the snapshots. At large values of ε_{LJ} a single pearl (intramolecular starlike micelle) is observed.

Figure 9 shows snapshots of a selected polymer with low density of grafts (side-chain length $m = 5$ and spacer length $n = 6$). Such polymers are expected to exhibit a pearl-necklace structure at moderate values of ε_{LJ} and undergo a transition to a unimolecular cylindrical micelle upon an increase in ε_{LJ}, which is also observed in the snapshots. For convenience, below we discuss the simulation results for graft copolymers with high and with low grafting densities in separate sections.

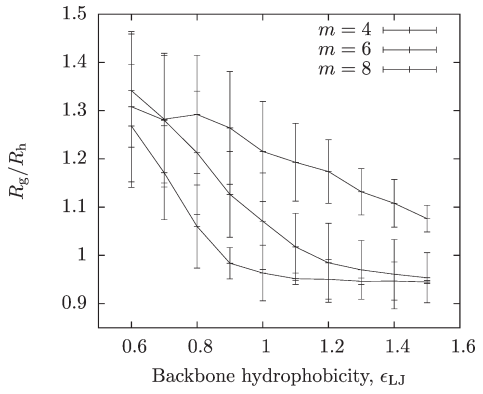

Figure 6. Variation of the ratio R_g/R_h with the change of the solvent quality for the backbone (ε_{LJ}, eq 2) for copolymers with low density of grafts (see Table 1).

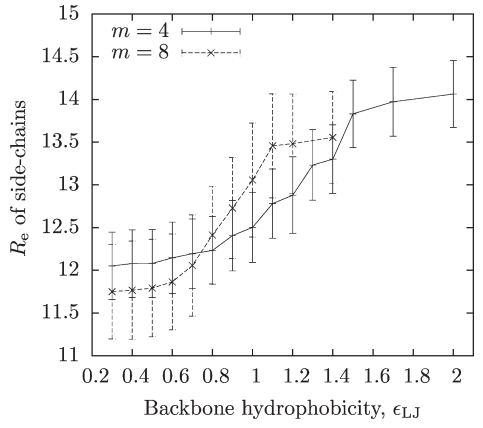

Figure 7. Variation of the end-to-end distance, R_e, of the side chains as a function of the solvent quality for the backbone (ε_{LJ}, eq 2) for systems with high density of grafts (see Table 1).

Copolymers with High Grafting Density: Starlike Intramolecular Micelles. In Figure 10 the average number of pearls in the backbone as a function of its hydrophobicity is plotted for the copolymers with high grafting density: $n = 40$, $m = 4$ and $n = 40$, $m = 8$ (see also Table 1). To identify the pearls and calculate their size, we use the algorithm of Limbach et al.[11] The number of pearls in the backbone calculated by this algorithm can be identified with the number of intramolecular micelles.

As discussed in the Theory section, the onset of the pearl formation occurs at certain poor solvent conditions for the main-chain monomers that corresponds in terms of our computational model to a certain value of $\varepsilon_{LJ} > \varepsilon_{LJ}(\theta) = 0.34$. In line with the predictions of the theory, we find that the number of pearls decreases with increasing ε_{LJ} in the range of intermediate and large ε_{LJ} values. Since the backbone length is constant and most of its material is in the pearls, decrease in their number implies simultaneous increase in their size. At a given value of ε_{LJ} the number of pearls decreases (that is, the number of spacers in each pearl increases) as a function of spacer length, m, in line with prediction of eq 26. We remark that qualitatively similar behavior has been observed for the copolymers with low density of grafts (Figure 13) which are discussed in the following section.

In the limit of large ε_{LJ}, corresponding to strong hydrophobicity of the main chain, the number of intramolecular micelles decreases, approaching a certain limiting value which in simulations is found to be equal to or larger than unity, depending on the length of the spacers, m.

The derivation of scaling relations for the aggregation number, p (eq 26), and for the size of the hydrophobic domains, eq 27, as a function of m and solvent quality conditions is based on the assumption of Gaussian elasticity of the spacers stretched in the radial direction inside the collapsed domains. This approximation is applicable as long as $R_{core} \leq m/2$. The hydrophobic units of the backbone fill the volume of the pearl while the side chains are pulled outside into the corona. As a result, the branch points are located at the surface. This implies that when $R_{core} \sim m/2$ the spacers in the pearls are stretched almost to the limit of their extensibility. In this regime the scaling relations, eqs 26 and 27 are not directly applicable. To estimate the pearl size in the regime when the spacer is strongly stretched, one can use geometrical arguments. At a given spacer length m, we assume that the radius of the pearl must satisfy $R_{core} \leq m/2$. Note that this condition is actually too strict, especially for low m, because it does not take into account the roughness of the surface of the small pearl as well as the fact that the segment does not have to be placed exactly in the center of the pearl, the fact that the pearl does not have to be exactly

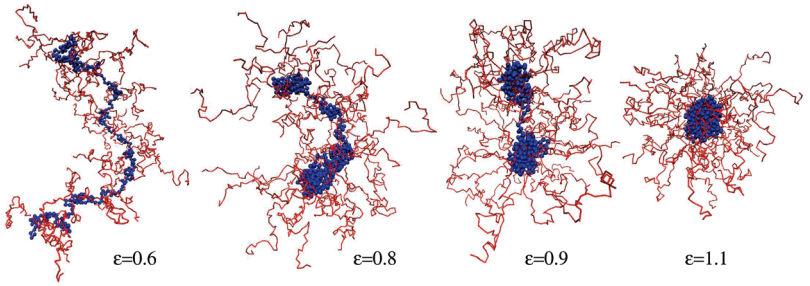

Figure 8. Simulation snapshots of the polymer with high density of grafts and the spacer size of $m = 8$ monomers illustrate the pearl-necklace transition with decreasing solvent quality (increasing ε_{LJ}) for the backbone. To make the structure of the backbone clearly visible, the side chains are only drawn as thin lines. Also for better visibility, magnification of the polymers slightly increases from left to right. In reality, the size of a segment is identical for all the polymers. Colors: backbone, blue; side chains, red.

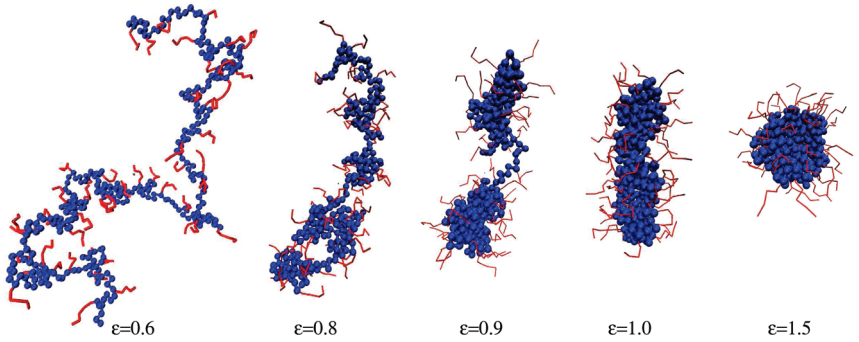

Figure 9. Simulation snapshots of the polymer with low density of grafts and the spacer size of $m = 6$ monomers illustrate the transition from a wormlike structure through a cylindrical micelle down to a spherical micelle with decreasing solvent quality (increasing ε_{LJ}) for the backbone. To make the structure of the backbone clearly visible, the side chains are only drawn as thin lines. Also, for better visibility, magnification of the polymers slightly increases from left to right. In reality, the size of a segment is identical for all the polymers. Colors: backbone, blue; side chains, red.

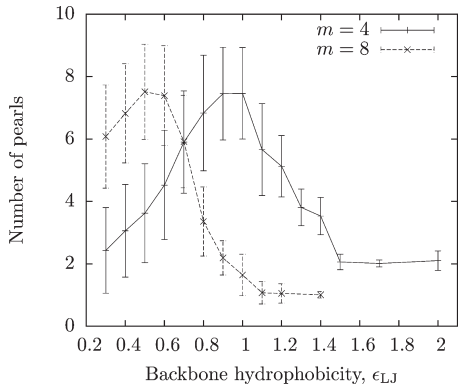

Figure 10. Number of aggregates (pearls) on the backbone as a function of ε_{LJ} for the copolymers with high density of grafts.

spherical, etc. Nevertheless, we can estimate the volume of the largest possible pearl as $V_{max} = {}^4/_3\pi({}^m/_2)^3$. Recalling that the diameter of the monomer unit is our unit of length, we can calculate the volume of a single monomer unit, $v = {}^4/_3\pi({}^1/_2)^3$. Then we can calculate the maximum number of monomer units in a pearl for a given spacer length as

$$n_{p,max} \approx y\frac{V_{max}}{v} = ym^3 \qquad (32)$$

where y is the packing fraction of monomer units. For hard spheres, the maximum possible packing fraction is $y = 74\%$. In the simulated systems we have soft spheres, but still it is reasonable to assume that $y \leq 1.0$. From eq 32, the maximum possible aggregation number of the micelles, p_{max}, can be expressed as

$$p_{max} \approx n_{p,max}/m \approx ym^2 \qquad (33)$$

Upon a decrease in the solvent quality for the monomer units of the main chain, the number of spacers in a pearl will grow asymptotically approaching the maximum value of $p \approx p_{max}$. For a given backbone length, N_b, the number of pearls on the polymer will be given as $N_b/n_{p,max}$. Hence, for a sufficiently long backbone, we get $N_b/n_{p,max} \gg 1$; i.e., in the limit of high ε_{LJ} (very poor solvent) the polymer will end up in a conformation comprising multiple pearls.

If we apply the calculations of the previous paragraph to the simulated polymers, taking $y \approx 1$, for $m = 8$ and $N_b = 320$ we get $N_b/n_{p,max} \approx 0.625 < 1.0$. The simulation results (Figure 10) show that indeed this polymer forms a single pearl at high values of ε_{LJ}. On the other hand, for $m = 4$, the same calculation yields $N_b/n_{p,max} \approx 5$, whereas Figure 10 shows that at high ε_{LJ} the polymer forms two pearls. This suggests that in reality the maximum pearl radius is slightly larger than $R_{core} = m/2$, which is in agreement with our expectations. Nevertheless, the results clearly show that for a given spacer length, m, a certain maximum pearl size exists and a densely grafted copolymer with sufficiently long backbone forms in the limit of high ε_{LJ} (very poor solvent) a chain of multiple intramolecular micelles.

The geometrical limitations to the pearl size grow with the cube of the spacer length. Therefore, the geometrical limitations to the pearl size are significant only for relatively short spacers. The same calculation for spacers of $m = 8$ and $m = 10$ yields that the limit of extension would be achieved only in the pearl composed of about 1400 and 2700 units, respectively. Since only relatively short graft copolymer chains were simulated, for $m \geq 8$ the number of grafts in the optimal micelle at $\varepsilon_{LJ} \rightarrow 2$ is equal to or larger than the overall number of grafts in the chain. Therefore, in the range of strong hydrophobicity of the main chain, $\varepsilon_{LJ} \rightarrow 2$, the whole copolymer molecule collapses into one starlike intramolecular micelle.

At low values of ε_{LJ} both plots in Figure 10 show that the algorithm counts the number of pearls as an increasing function of ε_{LJ}. In the detection algorithm we set the minimum detectable pearl size to 10 segments. Therefore, all aggregates smaller than this size are below the detection limit and are not counted. Setting a smaller detection limit is hardly possible because smaller pearls cannot be unambiguously identified. As one can see from the error bars in Figure 10, in the range of low ε_{LJ} the number of detectable pearls is strongly fluctuating. When one follows several simulation snapshots in a row, it can be noticed that pearls appear and disappear repeatedly, being destroyed by thermal fluctuations. In this range of ε_{LJ} the majority of the main chain monomers are not yet included in the pearls, and an increase in the pearl number is accompanied by their growth. This is in contrast with the behavior at large ε_{LJ} where most of the main-chain monomer units are in the pearls, and thus an increase in the aggregation number implies a decrease in the pearl number.

We remind the reader that scaling theory predicts formation of intramolecular micelles with finite aggregation number within a narrow range of variation of the solvent quality near the transition point. Hence, the theory predicts a nonmonotonous variation of the number of pearls in the chain as a function of (decreasing) solvent quality: a sharp increase in the number of pearls near the critical point $\tau \cong \tau_c$ is followed by a continuous decrease in the number of pearls upon further decrease in the solvent quality. A similar effect

of the finite size (single) pearl nucleation occurs in a chain stretched by external force upon a continuous decrease in the solvent strength.[29] Obviously, no scaling regime characterized by an increase in the number of pearls as a power law function of the solvent quality can be identified.

More precise analysis of the process of the pearl nucleation in the main chain is beyond the accuracy of the scaling approximation. Hence, we can conclude that strong fluctuations and smooth increase in the apparent number of pearls as a function of ε_{LJ} is a signature of the process of the pearl nucleation and a manifestation of strong fluctuations in the main-chain conformation near the transition point.

The position of the maximum in the number of detectable pearls as a function of ε_{LJ} may be considered as an upper estimate for the transition point $\varepsilon_{LJ,c}$. Upon an increase in the grafting density a shift of the position of the maximum toward larger values of ε_{LJ} is observed which is in agreement with the theoretical predictions, eq 13.

Detailed information about evolution of the number of the intramolecular micelles and about local conformation of the graft copolymers can be obtained from the plots of the bond angle cosines. We define the ensemble-averaged bond angle cosine for the ith bond angle, $\cos(\theta_i)$, as

$$\langle \cos(\theta_i) \rangle = \langle \vec{r}_i \cdot \vec{r}_{i+1} \rangle \qquad (34)$$

where $\vec{r}_i$ is the bond vector between the ith and $(i + 1)$st monomer unit. Both vectors are normalized to unit length. The angular brackets denote ensemble averaging. The meaning of the angle θ is illustrated in Figure 11.

The analysis of bond angle cosines as functions of bond positions, i, enables us to study the local extension of the chains. Thus, we can distinguish between expanded and collapsed domains within a single molecule. For a monomer unit inside a collapsed domain, the bond angle can take all values with approximately the same probability; only the excluded volume interaction forbids some values of θ close to 180°, as indicated in Figure 11a. Hence, in a collapsed domain the $\langle \cos(\theta_i) \rangle$ averages out to a value close to zero. On the other hand, for a monomer unit in a stretched domain, the angle θ is small, and hence the $\langle \cos(\theta_i) \rangle$ has an average value significantly higher than zero. This is schematically shown in Figure 11b. If a monomer unit is located in a place where the chain turns back forming a loop, the $\langle \cos(\theta_i) \rangle$ averages out to a value below zero as illustrated in Figure 11c.

The plots of bond-angle cosines are shown in Figure 12 for polymer with $m = 4$ and $n = 40$. The top graph for $\varepsilon_{LJ} = 0.6$ shows a highly stretched backbone without signs of pearls close to chain ends. Although in Figure 10 we can see that some pearls are supposed to be present in this system, they are presumably not well localized and smeared out by thermal fluctuations. The middle graph in Figure 12 shows the same polymer under much poorer solvent quality $\varepsilon_{LJ} = 1.4$. According to Figure 10, this polymer forms about three pearls (on average). The undulations in the middle graph of Figure 12 can be attributed to the stretched parts of the backbone forming the two bridges. The average number of pearls of this polymer, however, is slightly larger than 3, which suggests that it might exhibit some fluctuations in shape (frustration). Indeed, we have observed such large fluctuations in shape (frustration) in this polymer. Most of the time this system is present in the form of three pearls, but occasionally the central pearl splits into two smaller pearls. They are best illustrated by a simulation movie which is provided as Supporting Information.[38] It can be also noticed that the central pearls are much smaller than the pearls at the

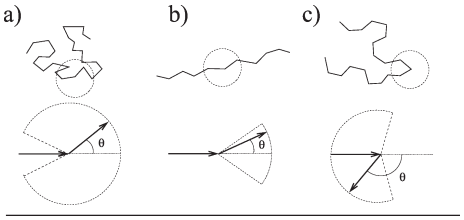

Figure 11. Illustration of the angle θ in eq 34 and its relation to the conformation. Part of the chain in a globular conformation (a), part of the chain that is stretched (b), and a part of the chain which turns back forming a loop (c). The most probable positions of the second bond vector are indicated by dotted lines.

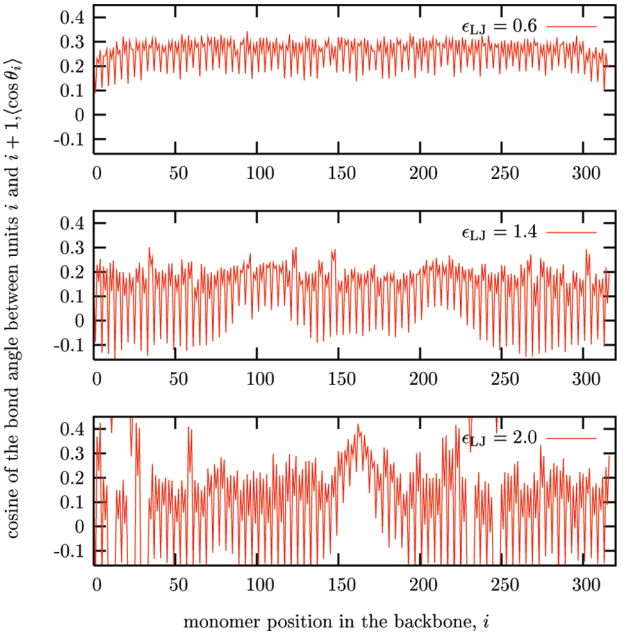

Figure 12. Cosine of the bond angle ($\langle \cos(\theta_i) \rangle$) in eq 34 as a function of monomer position in the chain for different values of ε_{LJ} for the polymer with high density of grafts, $n = 40$; $m = 4$. In the top graph ($\varepsilon_{LJ} = 0.6$) the chain is fully extended, in the middle one ($\varepsilon_{LJ} = 1.4$) it forms 3 pearls with 2 extended spacers, and in the graph at the bottom ($\varepsilon_{LJ} = 2.0$) two pearls and one spacer can be identified.

ends; i.e., the polymer responds to frustration also by forming pearls of other than the optimum size, p_{opt}. This is also the reason why the presence of the central pearl in the middle graph of Figure 10 is not well pronounced. Finally, the most clearly manifested presence of localized stretched part of the backbone can be observed in the bottom graph of Figure 12, which corresponds to polymer with a very hydrophobic backbone, $\varepsilon_{LJ} = 2.0$, forming two well-defined pearls. A detailed inspection of the plots of the bond-angle cosines shows that they have pronounced spikes at regular intervals which correspond exactly to the graft spacing. These spikes acquire negative values in the range where the pearls are formed, whereas in bridges they almost disappear. Recalling the discussion of the bond-angle cosines, we know that the negative values correspond to a chain turning back and forming a loop. This observation can be explained so that while the central parts of the spacers form the bulk of the pearls, at the grafting point, the spacer has to go to the surface of the pearl. This is most pronounced in pearls, radius of which is close to the limiting value $m/2$.

Copolymers with Low Density of Grafts: Morphological Transitions in the Intramolecular Micelles. Figure 13 shows the number of hydrophobic domains as a function of the

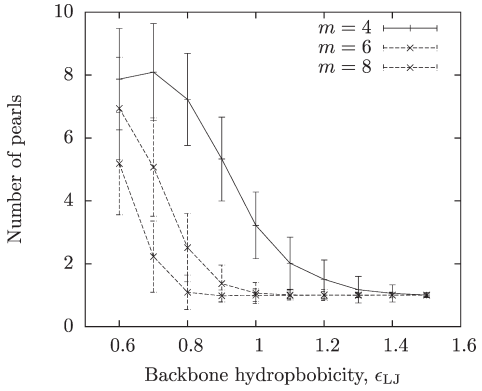

Figure 13. Average number of pearls as a function of hydrophobicity of the backbone, ε_{LJ}, for copolymers with low density of grafts and different lengths of the spacer, m.

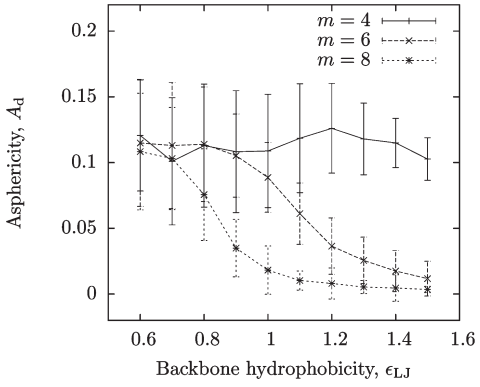

Figure 14. Asphericity of the conformation of the backbone as a function of its hydrophobicity, ε_{LJ}, for copolymers with low density of grafts and different lengths of the spacer, m.

hydrophobicity of the backbone, ε_{LJ}, for the systems with low grafting density. Data for several copolymers with fixed length of the grafts $n = 5$ and different spacings between the grafts, $m = 4$, 6, 8, are shown (see also Table 1 for polymer architectures).

As a general trend one can observe that with increasing ε_{LJ} the number of hydrophobic domains decreases down to the value of unity attained at sufficiently large ε_{LJ} for all the copolymers considered here. For larger spacers, the collapse occurs at lower values of ε_{LJ} than for the smaller spacers, again in agreement with the theory.

Information about the deviation from spherical symmetry can be obtained from asphericities of conformations. The asphericity is defined as[39]

$$A_d = \frac{1}{d(d-1)} \sum_{\alpha=1}^{d} \frac{(q_\alpha - \overline{q})^2}{\overline{q}^2} \tag{35}$$

where q_α are individual eigenvalues of the gyration tensor, $\overline{q}$ is their arithmetic mean, and $d = 3$ is the space dimensionality. For a sphere, $A_d = 0$, whereas it attains a maximum value of $A_d = 2/3$ for a collinear conformation.

The asphericities of the same copolymers as in Figure 13 are shown in Figure 14. Comparison of the two figures indicates that for the spacer length $m = 4$ the structure adopted at high value of ε_{LJ} is not spherical even though from Figure 13 it is clear that for $\varepsilon_{LJ} \geq 1.4$ it contains only one collapsed domain. Looking back at the snapshots in Figure 9, we can see that indeed the backbone collapses into a single globule which adopts a cylindrical shape. For the systems with spacer of $m = 6$ and $m = 8$ the asphericity approaches zero at high values of ε_{LJ}, indicating that they adopt spherical conformation.

In order to rationalize this behavior, we remind the reader that in cylindrical crew-cut micelles the radius of the core scales as[18]

$$R_{cyl} \cong \frac{m}{\tau} \left(\frac{\gamma}{n v^{1/3}} \right)^{6/11} \tag{36}$$

whereas the axial distance per graft is

$$h_{cyl} \cong \frac{\tau}{m} \left(\frac{n v^{1/3}}{\gamma} \right)^{12/11} \tag{37}$$

Hence, an increase in the spacer length m leads to a rapid increase in the radius and a decrease in the axial length of the cylindrical core of the intramolecular micelle. As a result, intramolecular micelles formed by sparsely grafted copolymers with sufficiently short main chain adopts symmetrical quasi-spherical shape, while for observation of cylindrical intramolecular aggregates simulations of much longer graft copolymers are needed.

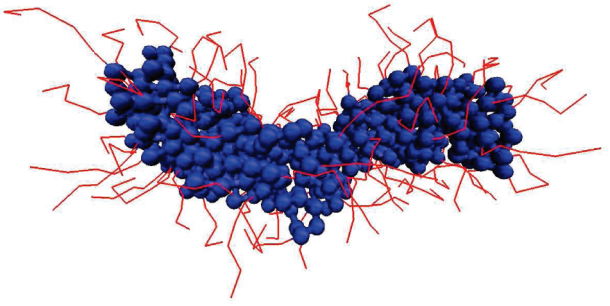

Figure 15. Simulation snapshot of a polymer with backbone length of $N_b = 500$ units, spacer $m = 6$, and graft length $n = 5$ provided to prove that for long enough backbones cylindrical conformation is obtained.

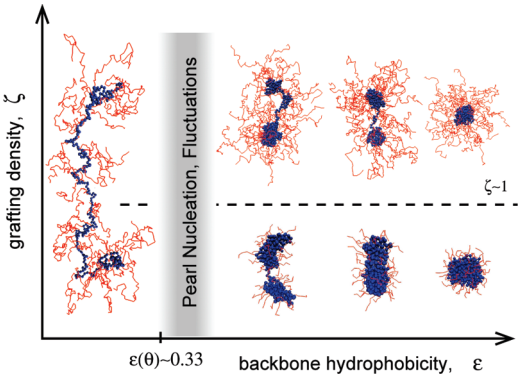

Figure 16. Schematic phase diagram showing different conformations of comb copolymers in selective solvents. The horizontal line $\zeta = 1$ separates the polymers with high ($\zeta > 1$) and low ($\zeta < 1$) grafting density. The spherical structures in the very poor solvent regime are attained only for short enough backbones.

As a proof of the concept, in Figure 15 we present snapshots from a simulation for a polymer with a longer backbone of $N_b = 500$ graft spacing $m = 6$ and the graft length $n = 5$. We have not performed a whole series of simulations for systems with such long backbones because the necessary computer time increases steeply with the size of the collapsed domain. To show that in this case the conformation is stable

and it is not only a carefully chosen fluctuation, we also provide a short simulation movie as Supporting Information.[40]

V. Conclusion

Molecular dynamics simulations of amphiphilic nonionic graft copolymers with variable intramolecular hydrophilic/hydrophobic balance qualitatively confirm the predictions of the scaling theory of the intramolecular conformational transitions and structure formation in such copolymers.[18] Moreover, combination of the simulations and the scaling approach provided results which are beyond the capabilities of each of these methods alone, such as finite-size effects and frustration behavior of real copolymers. In Figure 16 we present a schematic phase diagram, which summarizes the results of our simulations and outlines the main trends in the evolution of the intramolecular structures as a function of the copolymer architecture (grafting density) and the backbone hydrophobicity.

In particular, we have shown that collapse of the main chain in the densely grafted copolymers leads to the formation of a necklace of intramolecular starlike micelles with hydrophobic corelike domains (pearls) connected by extended bridges and hydrophilic (lyophilizing) corona formed by the grafts.

For the copolymers with the same length of grafts, the onset of the pearl-necklace formation is systematically shifted to smaller ε_{LJ} values (better solvent quality) upon an increase in the number of monomer units in the spacer.

Scaling analysis predicts that the formation of the finite-size intramolecular micelles occurs in a narrow interval of variation of the main-chain hydrophobicity near the transition point and is followed by a smooth increase in the aggregation number. The latter trend is confirmed by simulations. A more detailed analysis of the nucleation of pearls in the main chains is, unfortunately, beyond the resolution of both the scaling analysis and the pearl-counting algorithm used in our calculation.

The evolution of the number of intramolecular micelles as a function of variable hydrophobicity of the main-chain monomers and as a function of the spacer length was monitored using a special algorithm of counting the number of the hydrophobic collapsed domains (pearls).[11] The simulation results confirm the theoretical predictions that the average number of the micelles per copolymer molecule decreases while the average number of the main-chain monomers forming the core of the intramolecular micelle increases with increasing hydrophobicity of the main chain. For a given value of ε_{LJ} the number of micelles in the chain decreases as a function of the spacer length m.

When the number of micelles in the chain is small, it may be impossible to split the chain into equal micelles with aggregation number close to the optimum (corresponding to the minimum free energy per spacer). Here the system may become frustrated between configurations which differ by one intramolecular micelle but correspond to similar free energies. In this case the relative fluctuations in the size of the copolymers become of the order of unity. This type of frustrated behavior is observed in simulations in the range of ε_{LJ} when graft copolymers form two to four intramolecular micelles.

For the sparsely grafted copolymers with relatively long spacers, $m > n$, our simulations have unambiguously indicated, in a certain range of parameters, formation of cylindrical unimolecular micelles, in agreement with theoretical predictions. Moreover, the transition from the necklace of spherical intramolecular micelles to a cylindrical unimolecular micelle has been observed. As shown in our simulations and supported by theoretical arguments, this transition may occur upon a decrease in the solvent quality for the main-chain monomers. The asymmetrical cylindrical intramolecular micelles are well observed only for copolymers with sufficiently long backbones. For the copolymers with shorter backbones ($N_b = 320$, the same spacer length, m, and side-chain length, n) the intramolecular aggregates exhibit even at large ε_{LJ} only weakly asymmetric (quasi-spherical) shape.

Acknowledgment. This work was supported by the Marie Curie Research and Training Network (Grant No. 505 027 "Polyamphi"), by the Grant Agency of the Czech republic, Grant 203/05/H001, Grant Agency of the Academy of Sciences of the Czech Republic, Grant IAA400500703; by the Ministry of Education, Youth and Sports of the Czech Republic, Grant MSM0021620857, by the Russian Foundation for Basic Research (Grant RFBR 08-03-00336), and by the bilateral cooperation program BARRANDE 2009 between France and Czech Republic. The computer time was provided by the METACentrum computing facility under the research plan MSM6383917201.

Supporting Information Available: Simulation movies of a frustrated polymer and a cylindrical conformation for $N_b = 500$. This material is available free of charge via the Internet at http://pubs.acs.org.

References and Notes

(1) Zhang, M.; Muller, A. H. E. *J. Polym. Sci., Part A: Polym. Chem.* **2005**, *43*, 3461–3481.
(2) Bolisetty, S.; Airaud, C.; Xu, Y.; Muller, A. H. E.; Harnau, L.; Rosenfeld, S.; Linder, P.; Ballauff, M. *Phys. Rev. E* **2007**, *75*, 040803.
(3) Birshtein, T. M.; Borisov, O. V.; Zhulina, E. B.; Khokhlov, A. R.; Yurasova, T. A. *Polym. Sci. USSR* **1987**, *29*, 1293.
(4) Hsu, H.-P.; Paul, W.; Binder, K. *Macromol. Theory Simul.* **2007**, *16*, 660.
(5) Fredrickson, G. *Macromolecules* **1993**, *26*, 2825.
(6) Rouault, Y.; Borisov, O. V. *Macromolecules* **1996**, *29*, 2605.
(7) Feuz, L.; Leermakers, F. A. M.; Textor, M.; Borisov, O. V. *Macromolecules* **2005**, *38*, 8891–8901.
(8) Borisov, O. V.; Birshtein, T. M.; Zhulina, E. B. *Polym. Sci. USSR* **1987**, *29*, 1552.
(9) Lecommandoux, S.; Checot, F.; Borsali, R.; Schappacher, M.; Deffieux, A.; Brulet, A.; Cotton, J. P. *Macromolecules* **2002**, *35*, 8878.
(10) Feuz, L.; Strunz,P.; Geue, T.; Textor, M.; Borisov, O. V.
(11) Limbach, H. J.; Holm, C. *J. Phys. Chem. B* **2003**, *107*, 8041–8055.
(12) Limbach, H. J.; Holm, C. *J. Chem. Phys.* **2001**, *114*, 9674–9682.
(13) Košovan, P.; Limpouchová, Z.; Procházka, K. *Macromolecules* **2006**, *39*, 3458–3465.
(14) Košovan, P.; Limpouchová, Z.; Procházka, K. *J. Phys. Chem. B* **2007**, *111*, 8605–8611.
(15) Kramarenko, E. Y.; Pevnaya, O. S.; Khokhlov, A. R. *J. Chem. Phys.* **2005**, *122*, 084902.
(16) Pevnaya, O. S.; Kramarenko, E. Y.; Khokhlov, A. R. *J. Polym. Sci., Ser. A* **2007**, *49*, 1233–1241. *Eur. Phys. J. E* **2007**, *23*, 237−245.
(17) Aseyev, V. O.; Tenhu, H.; Winnik, F. M. *Adv. Polym. Sci.* **2006**, *196*, 1–85.
(18) Borisov, O. V.; Zhulina, E. B. *Macromolecules* **2005**, *38*, 2506–2514.
(19) Dobrynin, A. V.; Rubinstein, M.; Obukhov, S. P. *Macromolecules* **1996**, *29*, 2974–2979.
(20) Polotsky, A. V.; Charlaganov, M. I.; Xu, Y.; Leermakers, F. A. M.; Daoud, M.; Muller, A. H. E.; Dotera, T.; Borisov, O. V. *Macromolecules* **2008**, *41*, 4020–4028.
(21) Hugouvieux, V.; Axelos, M. A. V.; Kolb, M. *Macromolecules* **2009**, *42*, 392–400.
(22) Micka, U.; Holm, C.; Kremer, K. *Langmuir* **1999**, *15*, 4033.
(23) Binder, K., Ed. *Monte Carlo and Molecular Dynamics Simulations in Polymer Science*; Oxford University Press: New York, 1995.
(24) Grest, G. S.; Kremer, K. *Phys. Rev. A* **1986**, *33*, 3628–3631.
(25) Limbach, H.-J.; Arnold, A.; Mann, B. A.; Holm, C. *Comput. Phys. Commun.* **2006**, *9*, 704–727.
(26) http://www.espresso.mpg.de.
(27) de Gennes P. G. *Scaling Concepts in Polymer Physics*; Cornell University Press: Ithaca, NY, 1979.

(28) Halperin, A.; Zhulina, E. B. *Europhys. Lett*. **1991**, *15*, 417.
(29) Polotsky, A. A.; Charlaganov, M. I.; Leermakers, F. A. M.; Daoud, M.; Borisov, O. V.; Birshtein, T. M. *Macromolecules*, accepted.
(30) Pincus, P. *Macromolecules* **1976**, *9*, 386.
(31) (a) Daoud, M.; Cotton, J.-P. *J. Phys.* (*Paris*) **1982**, *43*, 531. (b) Birshtein, T. M.; Zhulina, E. B. *Polymer* **1984**, *25*, 1453.
(32) (a) Zhulina, E. B.; Birshtein, T. M. *Polym. Sci. USSR* **1985**, *27*, 570. (b) Halperin, A. *Macromolecules* **1987**, *20*, 2943.
(33) Halperin, A.; Alexander, S. *Macromolecules* **1987**, *20*, 1146.
(34) Borisov, O. V.; Zhulina, E. B. *Macromolecules* **2003**, *36*, 10029–10036.
(35) Zhulina, E. B.; Adam, M.; LaRue, I.; Sheiko, S.; Rubinstein, M. *Macromolecules* **2005**, *38*, 5330.
(36) Grosberg, A. Yu.; Khokhlov, A. R.*Statistical Physics of Macromolecules*; AIP Press: New York, 1994.
(37) We do not show the same plot for the simulated systems with low grafting density because their side chains are too short and the change in the end-to-end distance is too small to be well observable.
(38) Simulation movie of a frustrated polymer (Supporting Information).
(39) Jagodzinski, O.; Eisenrigler, E.; Kremer, K. *J. Phys.* (*Paris*) **1992**, *2*, 2243–2279.
(40) Simulation movie of a cylindrical conformation for $N_b = 500$ (can be downloaded from http://lynette.natur.cuni.cz/~kosovan/download/nn320_40_4_1.0_mov.mpg).